Mechanisms of Degradation of $Na_2Ni[Fe(CN)_6]$ Functional Electrodes in Aqueous Media: A Combined Theoretical and Experimental Study

Xaver Lamprecht[a], Iman Evazzade[b], Iago Ungerer[a], Ludek Hromadko[c,d], Jan M. Macak[c,d], Aliaksandr S. Bandarenka*[,a], Vitaly Alexandrov*[,b]

(a) - Physics of Energy Conversion and Storage, Physik-Department, Technische Universität München, James-Franck-Str. 1, 85748 Garching bei München, Germany

(b) - Department of Chemical and Biomolecular Engineering and Nebraska Center for Materials and Nanoscience, University of Nebraska-Lincoln, Lincoln, Nebraska 68588, United States

(c) - Central European Institute of Technology, Brno University of Technology, Purkynova 123, 61200, Brno, Czech Republic

(d) – Center of Materials and Nanotechnologies, Faculty of Chemical Technology, University of Pardubice, Nam.Cs.Legii 565, 53002 Pardubice, Czech Republic

* Corresponding Author Emails: valexandrov2@unl.edu; bandarenka@ph.tum.de

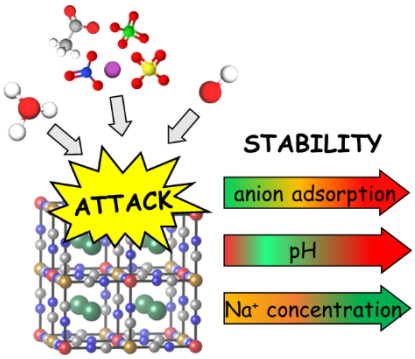

TOC Figure (5,5 x 5 cm)

TOC text (max 50 words)

The degradation mechanism of Prussian Blue Analogs strongly depends on the electrolyte composition. The solution pH, concentration and anion adsorption affinity are identified as the key parameters to influence the material stability.

Abstract

Prussian Blue Analogs (PBAs) are versatile functional materials with numerous applications ranging from electrocatalysis and batteries to sensors and electrochromic devices. Their electrochemical performance involving the long-term cycling stability strongly depends on the electrolyte composition. In this work, we use density functional theory calculations and experiments to elucidate the mechanisms of degradation of model $Na_2Ni[Fe(CN)_6]$ functional electrodes in aqueous electrolytes. Next to the solution pH and cation concentration, we identify anion adsorption as a major driving force for the electrode dissolution. Notably, the nature of adsorbed anions can control the mass and charge transfer mechanisms during metal cation intercalation, as well as the electrode degradation rate. We find that weakly adsorbing anions, such as NO_3^-, impede the degradation, while strongly adsorbing anions, such as SO_4^{2-}, accelerate it. The results of this study provide practical guidelines for the electrolyte optimization and can likely be extrapolated to the whole family of PBAs operating in aqueous media.

Keywords

Prussian blue analogs; sodium nickel hexacyanoferrate; transition metal dissolution; degradation; electrolyte effect; anion adsorption; density functional calculations

Introduction

Prussian Blue Analogs (PBAs) are widely used in different materials science disciplines, as they provide various functionalities for battery applications,[1,2,3,4] (electro)sensorics,[5,6] heterogeneous (electro)catalysis,[7,8,9] as well as electrochromic devices.[10] PBAs can be represented by the general formula $A_xTM^1[TM^2(CN)_6]$, where A is usually Li, Na or K, and TM is a transition metal such as Fe, Mn, Co, Ni or Zn. PBAs typically belong to the cubic space group *Fm-3m,* and the crystal structure is characterized by transition metals interconnected by C≡N bridges forming $TM(CN)_6$ octahedra.[4] Alkali metal cations can (de)intercalate through the three-dimensional channels in the structure. Owing to the high tunability of chemical composition, PBAs can be considered as model materials in coordination and inorganic chemistry, being analogs of the well-known metal-organic frameworks (MOFs).[11] Therefore, a basic understanding of the correlations between various functional properties of PBAs and their composition or structure is of great fundamental importance.

In the case of energy conversion and storage applications, the properties of electrified interfaces between electronically conducting PBAs and aqueous electrolytes are of central significance. So far, one fundamental property that has received very limited attention is the electrochemical stability of PBA-based electrodes. Most of the previous stability studies focused on how solution pH affects the degradation of PBA materials.[12,13,14,15,16] However, it was recently demonstrated that the degradation rate of aqueous sodium-ion battery electrodes based on PBAs strongly depends not only on solution pH, but also on the nature of anions present in the electrolytes.[17] Specifically, for the $Na_2Ni[Fe(CN)_6]$ and $Na_2Co[Fe(CN)_6]$ model electrodes, the transition-metal dissolution during charge-discharge cycles was recently monitored in real time using an inductively coupled plasma mass spectrometer. The study revealed distinct transition-metal dissolution patterns strongly correlated with the electrochemical potential and current. It was shown that the degradation rate increases in the order $ClO_4^- < NO_3^- < Cl^- < SO_4^{2-}$, revealing

almost no capacity loss after 10 000 cycles for $Na_2Ni[Fe(CN)_6]$ in highly concentrated $NaClO_4$. However, the atomistic mechanisms underlying such behavior remain unclear.

In this work, we combine experiments and density functional theory calculations to elucidate the properties of the electrified interface between model nickel hexacyanoferrate (NiHCF, $Na_2Ni[Fe(CN)_6]$ and $NaNi[Fe(CN)_6]$) electrodes and aqueous electrolytes in the presence of anions commonly used in electrochemical systems. A significant affinity of the PBA surface to anionic species explains the complex mechanism of the interfacial mass and charge transfer during intercalation of alkali metal cations and drastic differences in the stability of PBA materials in the presence of different anions.[18,19,20] It is found that surface Fe-sites are more favorable for anion adsorption than Ni-sites. Towards the edges of the pH scale, the initial stages of the electrode degradation involve the attack of Fe-sites by OH^- (at high pH) or protonation of the CN-groups of the crystal (at low pH). These findings should be of great importance for optimizing the electrochemical behavior of PBA-containing systems, interpreting experimental results, and refinement of advanced models of the electrified PBA/electrolyte interfaces.

Results and Discussion

Figures 1a and **1b** show the atomic structure of nickel hexacyanoferrate ($Na_2Ni[Fe(CN)_6]$) used in this study as a representative PBA to understand its degradation properties in aqueous electrolytes better. The recorded X-ray diffractometry (XRD) pattern of the electrodeposited thin-film (see **Figure 1c**) matches very well with the calculated pattern for the *Fm-3m* structure. The strong (200) reflection allows to calculate the lattice constant for the material yielding 10.28 Å. This value is in good accordance with the results of our DFT optimization (10.32 Å).

It is, therefore, reasonable to use the presented atomic structure for further DFT simulations of the processes at the electrified electrode-electrolyte interface. As visible from the SEM image in **Figure 1d**, the NiHCF thin-film obtained from the electrochemical deposition is characterized by a very homogenous coating on top of the Au substrate.

The electrochemical activity in PBAs is based on alkali metal ion, e.g., sodium, (de)intercalation accompanied by the corresponding redox reaction of the host transition metals. NiHCF has only Fe(II/III) as an active redox center since Ni species are electrochemically inert in the operating window of water-based electrolytes. The corresponding redox reaction is represented by

$$Na_2Ni^{II}[Fe^{II}(CN)_6] \text{ (intercalated)} \rightleftharpoons Na^+ + e^- + NaNi^{II}[Fe^{III}(CN)_6] \text{ (50\% deintercalated)} \quad \text{(Eq. 1)}$$

Indeed, our Bader charge analysis based on DFT calculations of the NiHCF slabs shows that Ni ions do not change their charge upon 50% deintercalation with q(Ni) = 1.30, whereas the positive charge on Fe ions increases from q(Fe) = 1.17 for the fully intercalated case up to 1.33 for the deintercalated case. This agrees well with an analysis of the density of states (DOS), revealing that the Fe electronic states below the Fermi energy for the intercalated material shift towards the Fermi level for the deintercalated material (**Figure 1e**).

This is further confirmed by X-ray photoelectron spectroscopy (XPS) measurements of oxidized and reduced electrodes, which were electrochemically brought to their respective final states. NiHCF was completely reduced at a potential of 0.1 V *vs*. SSC, whereas it was completely oxidized at 0.8 V *vs.* SSC. As seen in **Figure 1f**, the samples show strongly differing spectra in the Fe 2p region. For the intercalated electrode, one sharp peak, which is observed in both regions of the spin-orbit doublet, can be associated with the Fe^{II} oxidation state as expected for fully sodiated NiHCF. Upon deintercalation, Fe^{II} is oxidized to Fe^{III}, which is well represented by the appearance of an additional peak at higher binding energies in both doublet

regions.[21] On the other side, the spectra obtained for Ni 2p show identical peaks with regards to the corresponding binding energies and intensities, proving that Ni is electrochemically inert within the investigated potential window.

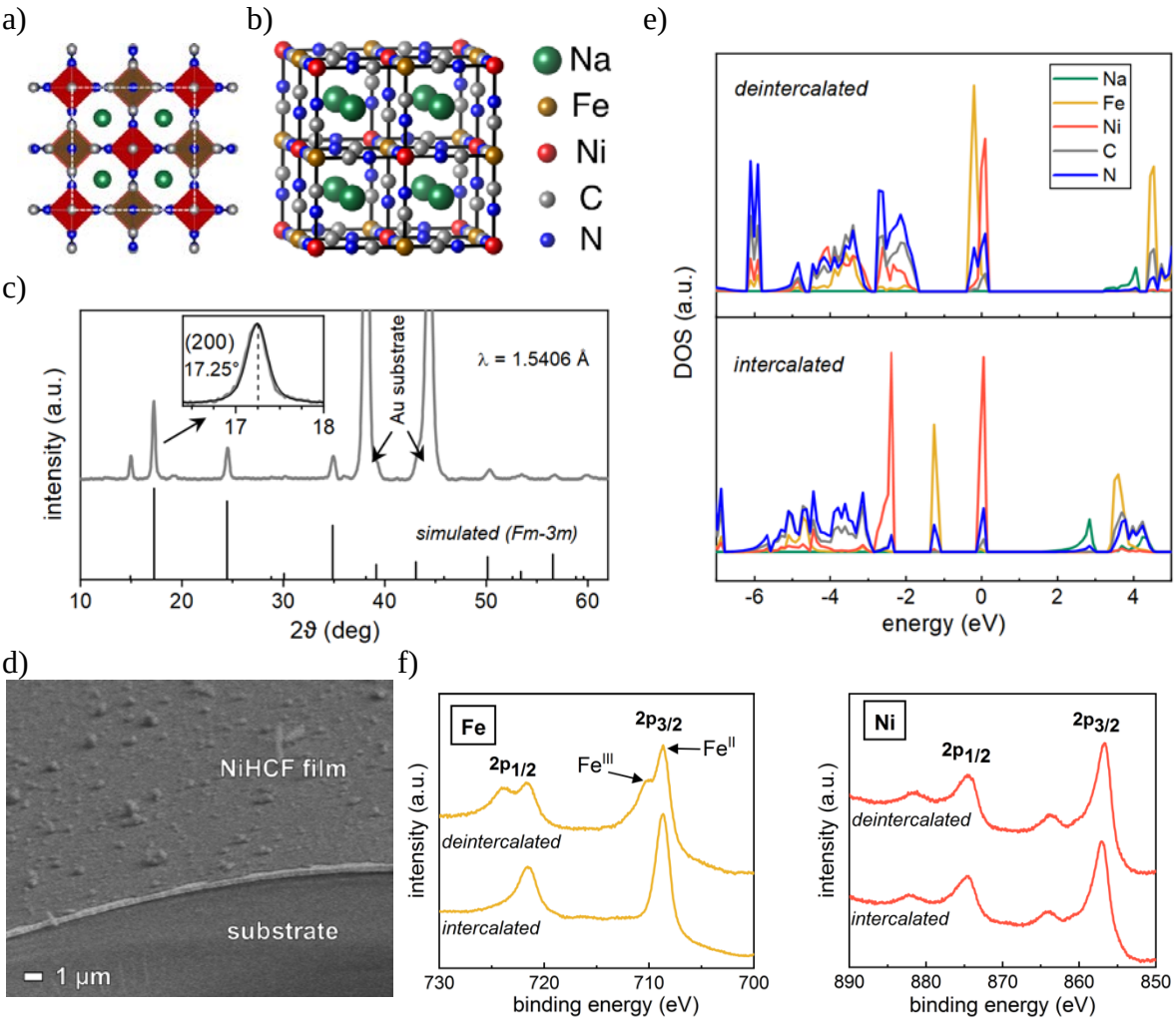

Figure 1. Polyhedral (a) and ball-and-stick (b) representations of the nickel hexacyanoferrate $Na_2Ni[Fe(CN)_6]$ crystal structure in the cubic space group *Fm-3m*. (c) XRD pattern of the NiHCF thin-film together with the simulated reflections for the crystal structure given in (b). SEM image of the electrodeposited thin-film electrode (d). (e) Density of states (DOS) for fully intercalated and 50% deintercalated bulk NiHCF. (f) XPS spectra showing the Fe 2p and Ni 2p regions for intercalated and deintercalated NiHCF.

The electrochemical oxidation (de-sodiation) and reduction (sodiation) of the NiHCF electrode in 0.25 M $NaClO_4$ results in a very sharp and reversible redox peak (see **Figure 2a**). **The** electrode mass change over one CV-cycle, as measured by EQCM, strictly follows the consumed charge (**Figure 2b**). By using the Faraday's law, a molar mass of 22.6 g mol^{-1} is obtained for the (de)intercalating species, from which it can be confirmed that the charge compensation is achieved by the transport of Na^+ ions across the electrode-electrolyte interface (**Figure 2c**).

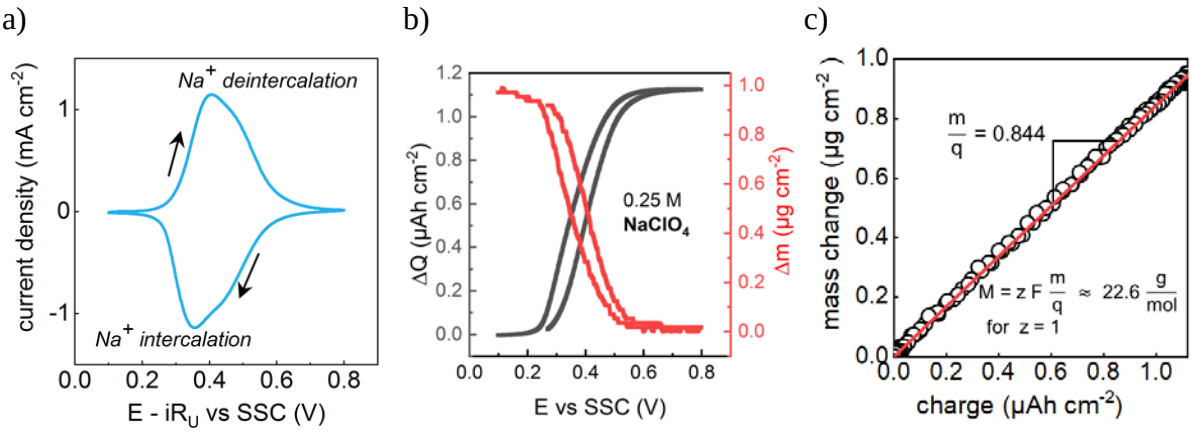

Figure 2. (a) Representative cyclic voltammogram of NiHCF in 0.25 M $NaClO_4$ showing the redox response of $Fe^{II/III}$ in the PBA complex. The electrode charge and mass change (b) during the forward and backward scan of the CV is correlated to Na^+ (de)intercalation by EQCM using the Faraday's law (c).

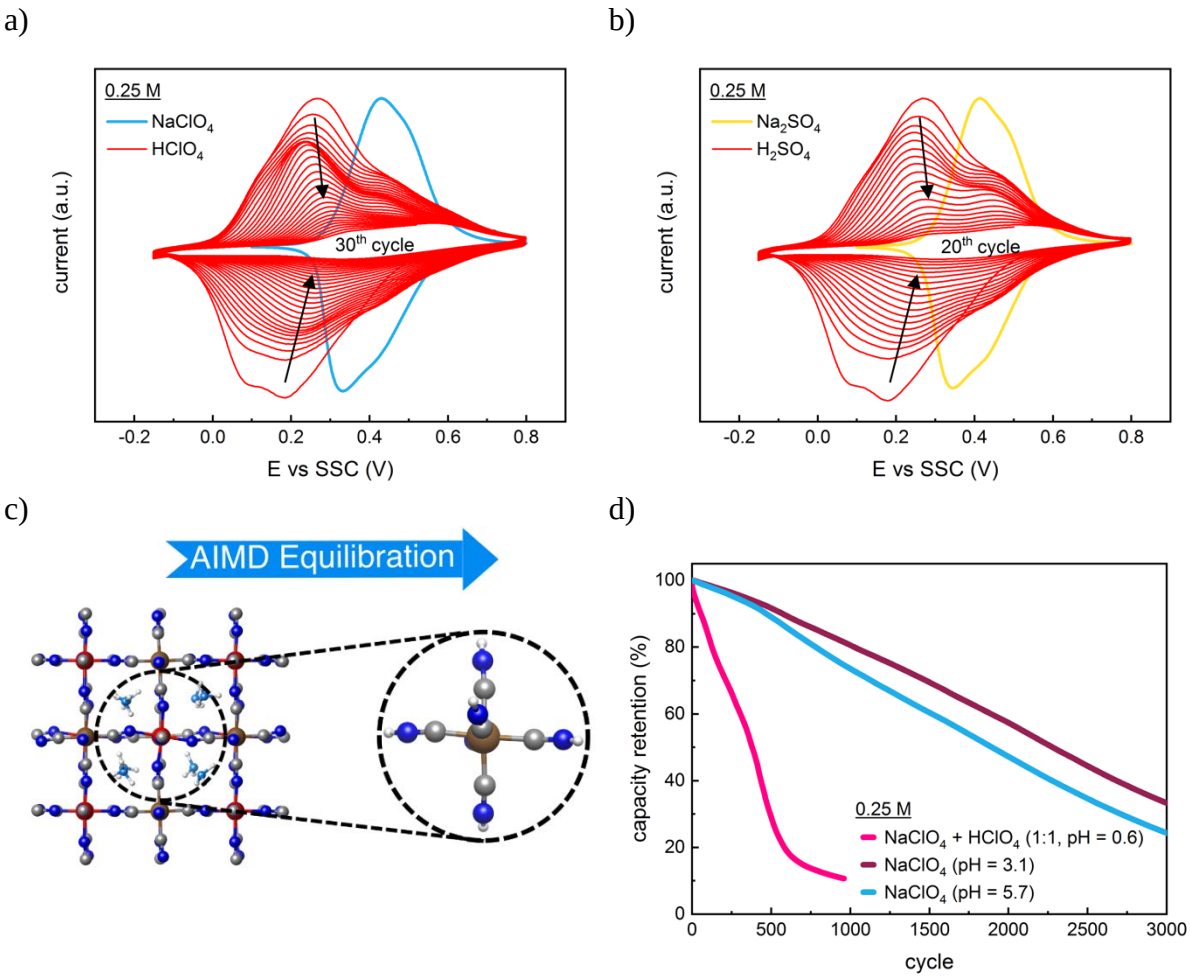

Figure 3. Fast degradation of NiHCF in (a) 0.25 M $HClO_4$ and (b) 0.25 M H_2SO_4 due to active material dissolution. (c) Ab initio molecular dynamics simulation predicts the cleavage of the $[Fe - C \equiv N] - Ni$ bond due to protonation of the N sites if Na^+ in NiHCF is replaced by H_3O^+. (d) Impact of the H^+ *vs.* Na^+ availability on the stability of NiHCF during galvanostatic cycling.

It was previously reported that the transition metal dissolution from NiHCF is highly dependent on solution pH and anions present in the electrolyte.[17] However, the NiHCF degradation mechanism as a function of electrolyte composition remains poorly understood. This study distinguishes two degradation regimes corresponding to acidic and alkaline aqueous electrolytes.

We first analyze the mechanism of active material degradation in acidic solutions in the absence of alkali metal cations. It can be assumed that at low pH, the most abundant cationic solution

species available for intercalation into the NiHCF structure are hydronium (H_3O^+) ions. An oxidized $NaNi[Fe(CN)_6]$ electrode was transferred to a 0.25 M $HClO_4$ solution and electrochemically cycled in the absence of Na^+ in the electrolyte (**Figure 3a**). Starting right from the first cycle, the material degrades severely, as visible from the rapidly decreasing current waves in the voltammogram. After less than 30 cycles, the redox activity has almost entirely vanished. Similarly, an instantaneous degradation was observed for de-sodiated NiHCF in 0.25 M H_2SO_4, which can be considered as completely degraded after already 20 cycles (**Figure 3b**). It should be noted that the potential range was extended towards lower potentials, as the redox peak was shifted for the acidic solutions compared to the Na^+ electrolytes. It has been reported that the nature of the intercalating cationic species strongly impacts the half-charge potential ($E_{1/2}$) of PBA materials, with $E_{1/2}$ decreasing when going up the periodic table from the large Cs^+ ion towards the small Li^+.[22,23] It is, therefore, reasonable that the intercalation of H_3O^+ in NiHCF is observed at potentials lower than that for Na^+.

Due to the highly decreased cycling stability of NiHCF in the Na^+-free acidic solutions compared to pH-neutral Na^+ electrolytes, it can be assumed that the intercalation of H_3O^+ is likely responsible for the fast structure destruction. To probe the acidic dissolution mechanism by a theoretical approach, we replace Na^+ cations in the NiHCF structure with H_3O^+ maintaining the same charge of the cell and run *ab initio* molecular dynamics (AIMD) simulations. Already after 1-2 ps of AIMD equilibration, we observe spontaneous protonation of the N sites resulting in the generation of $Fe(CN\text{-}H)_6$ moieties (see **Figure 3c**). This suggests that the N-sites are the primary point of attack in acidic electrolytes during the NiHCF degradation process. This should lead to the dissolution of $Fe(CN)_6^{3-}$ complexes, while the remaining Ni cations are expected to dissolve as solvated Ni^{2+} species.

Indeed, acidic solutions (mostly HCl) were used in previous studies to intentionally etch PBA derivates to transform precipitated microcrystals into a desired geometry for improved ion transport by creating nanoframes and hollow structures with large surface areas and beneficial pore volume properties.[24,25,26] Selective etching of such mesocrystals could be established by making use of the observation that crystal domains with a higher defect density, such as dangling ligand bonds, exhibited faster etching rates.[24,27] However, surfaces exposed to an acidic solution appeared to be protected from degradation by the co-solvation of polyvinylpyrrolidone (PVP), by which hollow PBA structures could be formed. It was assumed that the protection mechanism was enabled by the adsorption of PVP through its amide group on the surface-exposed Fe-sites, whereas protons diffused into the crystal and initiated the etching process from within.[26,28] In contrast to that, Wu *et al*. reported unexpectedly high cycling stability of a copper hexacyanoferrate (CuHCF) proton-insertion battery electrode even in 2 M H_2SO_4. However, the stability varied strongly among the investigated Cu-, Ni-, Co- and Mn-based PBA derivates.[29] In fact, the hydrated CuHCF crystals studied by them had an inherently high $Fe(CN)_6$ defect density, which were passivated by ligand H_2O molecules occupying the anionic site of the crystal structure. DFT calculations revealed that the most favorable binding sites for protons inserted into the structure were zeolitic water molecules within the interstitial sites of the crystal. On the other side, the ligand water was assumed to be strongly bound to the uncoordinated copper cations of the crystal *via* its oxygen atom, discouraging the formation of ligand hydronium. Nevertheless, an interconnected hydrogen bonding network along the zeolitic and ligand H_2O was assumed, allowing an extremely fast H^+ Grotthus-conduction mechanism. Apparently, competing effects based on the hydration state and defect density of the crystals, as well as the surface adsorption of large molecules, can strongly impact the proneness of PBAs to proton attack.

Overall, acidification of Na^+-containing electrolytes is a well-established strategy to enhance the stability of PBAs in aqueous media.[13,17,30,31] This is represented in **Figure 3d**, where the reduction of the pH of $NaClO_4$ from its initial value of pH = 5.7 to pH = 3.1 *via* the addition of $HClO_4$ leads to a significant decrease of the degradation rate during galvanostatic cycling. The reason for the higher stability of PBAs in slightly acidified electrolytes is caused by the absence of OH^-. In short, abundant hydroxide species (represented by a high pH value) are known to initiate the almost immediate degradation of PBA materials due to the entire extraction of $[Fe(CN)_6]^{3/4-}$ and subsequent formation of surface-confined NiO_x.[17] If the electrolyte is however strongly acidified with an equal concentration of 0.25 M $HClO_4$ and $NaClO_4$, the NiHCF electrode degradation is extremely accelerated, whereas it is still more stable compared to the pure 0.25 M $HClO_4$ solution (**Figure 3a**). From this, we conclude that NiHCF has a higher affinity for Na^+ insertion compared to H_3O^+, and the stabilization is caused by the reduced co-insertion of hydronium when Na^+ ions are available as an intercalate. Therefore, the use of slightly acidified Na^+ electrolytes (to pH ≈ 3) should serve as a very effective strategy to enhance the stability of PBA electrodes due to the practical absence of OH^-, while still providing a high Na^+:H_3O^+ ratio.

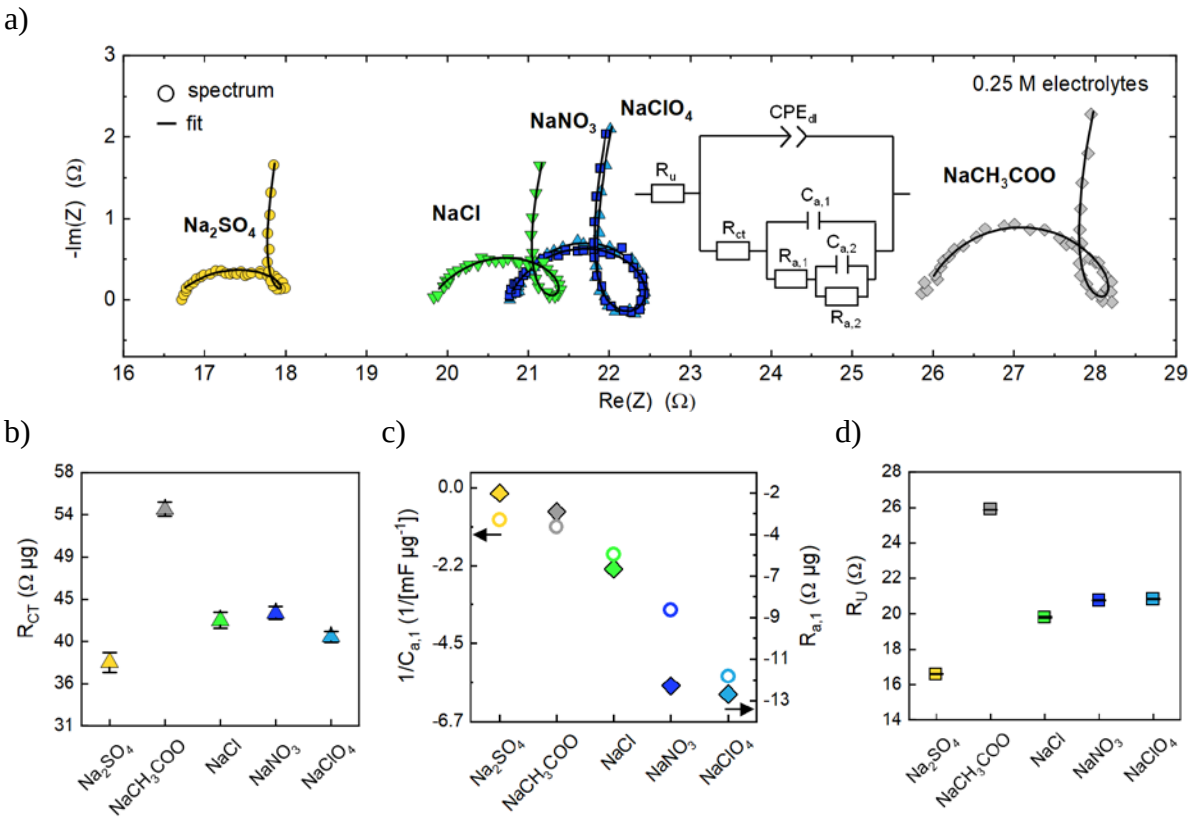

Figure 4. (a) Impedance spectra (at 0.4 V *vs.* SSC) of NiHCF recorded in 0.25 M Na^+ electrolytes with varying anion species. The impedance spectra were fitted using the displayed equivalent circuit yielding the extracted fitting parameters for R_{CT} (b), $1/C_{a,1}$ (hollow symbols, left axis) with $R_{a,1}$ (filled symbols, right axis) (c) and R_u (d).

For alkaline/neutral solutions, we investigate the role of a series of common anionic species on the degradation rate of PBA materials. It was shown by Yun *et al*. that electrolyte anions play a significant role in the interfacial charge and mass transfer processes for intercalation-type battery materials.[20] **Figure 4a** shows the impedance spectra for NiHCF in 0.25 M Na^+ electrolytes for varying anions, in particular ClO_4^-, NO_3^-, Cl^-, CH_3COO^- and SO_4^{2-}. Characteristic loop-shaped spectra were obtained for all electrolytes, which were fitted with the equivalent electric circuit displayed in **Figure 4a**. Next to the "classical" elements as the uncompensated resistance (R_u), a constant phase element (CPE) representing the double layer capacitance and the charge transfer resistance (R_{CT}) for faradaic currents, another superposition

of two RC elements ($R_{a,1}$, $C_{a,1}$, $R_{a,2}$, $C_{a,2}$) represents the intermediate adsorption of anions on the electrode surface during the alkali metal cation insertion process. This physical model describes the so-called “three-step mechanism” of intercalation. In short, the quick electron transfer on $Fe^{II/III}$ results in the appearance of uncompensated surface charges due to the considerably slower extraction or insertion of sodium from or into the crystal structure. This excess surface charge is compensated by the intermediate adsorption of the highly mobile electrolyte anions on the electrode surface.[18,19,20,32] From **Figure 4b,** it is apparent that the nature of the anions have, as expected, no significant impact on the charge transfer resistance and thereby the corresponding rate constants of the redox reaction, whereas the capacitance ($C_{a,1}$) and resistance ($R_{a,1}$) representing the anion adsorption strongly deviate among the different anions (**Figure 4c**). From this, we can conclude that the complex interfacial mechanism of alkali metal cation intercalation strongly depends on the respective adsorption affinity of the involved anions. The different ionic conductivities of the salt solutions are represented by the varying uncompensated resistance values (**Figure 4d**), which are nevertheless in a comparable range.

Following this argumentation, the anion nature should determine the electrochemical performance of PBA electrodes. **Figure 5a** shows the CVs of NiHCF in 0.25 M Na^+ electrolytes with ClO_4^-, NO_3^-, Cl^-, CH_3COO^- and SO_4^{2-} as the respective anionic species. The potential was corrected for the uncompensated resistance to eliminate any effects stemming from the different ionic conductivities of the solutions. Apparently, the peak shape and position are highly symmetric in all cases and remain unaffected from the present anion. Furthermore, the apparent molar mass of the intercalating species was determined to be very close to the expected 22.99 g mol^{-1} for all investigated electrolytes, showing that only sodium is inserted into the host structure (see **Figure S1**). From the consistently reversible CV curves, it can be concluded that all tested anionic species effectively compensate for the intermediate excess

surface charges during the redox process and that the corresponding adsorption and desorption steps proceed fast enough to not be rate limiting. While this process is supposed to be fully reversible in theory, we observed a significant impact from the involved anion on the electrode stability in our previous study.[17]

To correlate the degradation rates to the specific anions, we repetitively cycled NiHCF thin-film model electrodes in equally concentrated Na^+ electrolytes with comparable neutral pH = 5.7 – 6.2 as shown in **Figure 5b**. The electrode stability was found to decrease with the order of ClO_4^- > NO_3^- > Cl^- > CH_3COO^- > SO_4^{2-}, with the capacity retention after 2000 cycles ranging from 67% for perchlorate to only 5% for sulphate. This finding strongly indicates the detrimental role of some anions and their notable role in promoting electrode dissolution. The order of electrode stability as a function of the involved anion is also in great agreement with previous findings for other PBA materials, namely $NaIn[Fe(CN)_6]$ and $K_2Cr[Fe(CN)_6]$.[33,34] Besides, it is well known that PBA electrodes are entirely unstable in the presence of OH^-.[14,15,16] **Figure 5c** shows the almost immediate disintegration of NiHCF upon cycling in 0.1 M NaOH (pH = 13). As previously reported, the electrode degradation is characterized by an entire loss of $Fe(CN)_6^{3/4-}$ and the subsequent formation of surface-confined NiO_x phases, represented by the increasing current from the Ni(II/III) redox couple.[15,17]

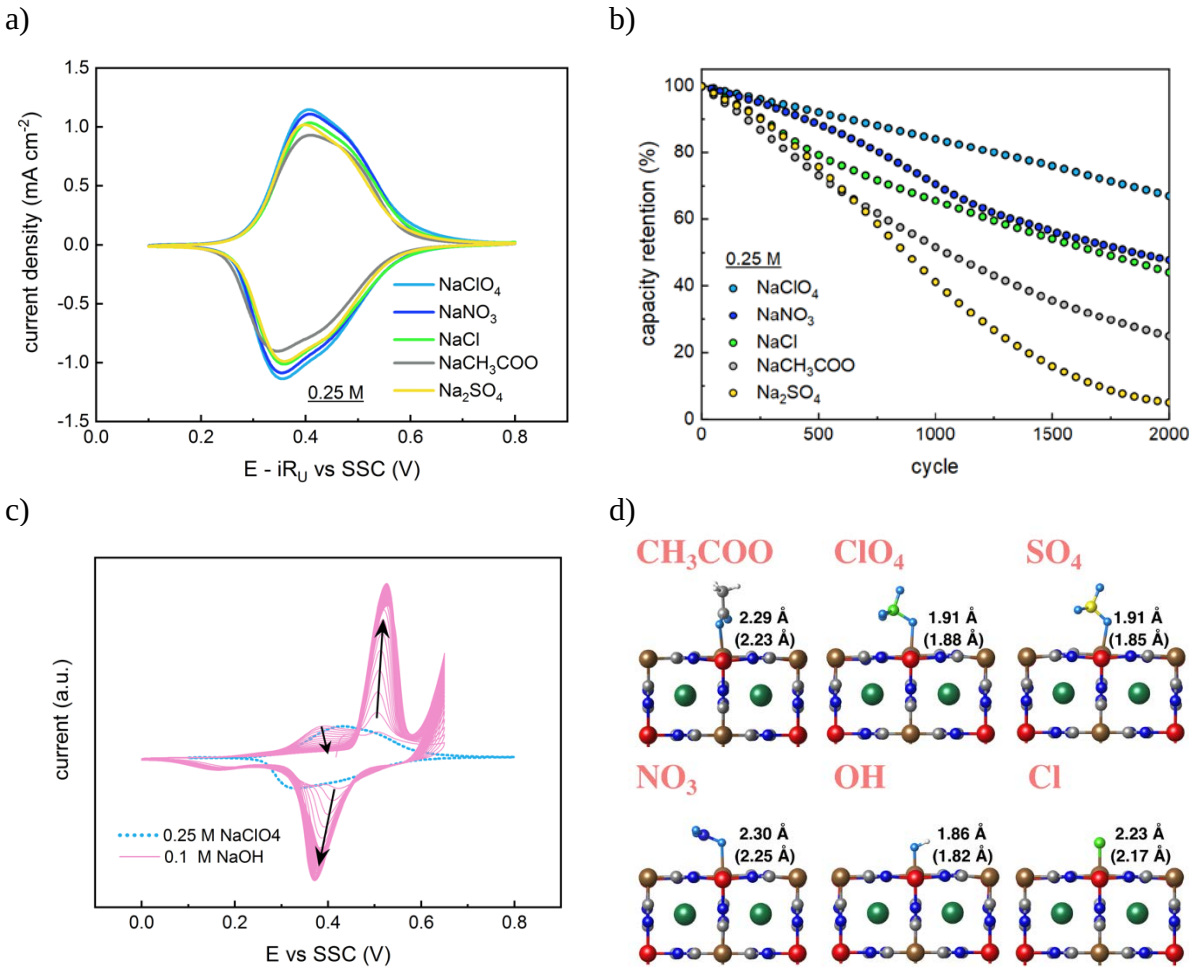

Figure 5. (a) Cyclic voltammograms (50 mV/s) and (b) cycling stability (galvanostatic oxidation and reduction at a rate of 300C) of NiHCF recorded in 0.25 M Na^+ electrolytes with varying anion species. (c) Fast degradation of NiHCF in 0.1 M NaOH due to the extraction of $Fe(CN)_6^{3/4-}$ and progressing formation of NiO_x. (d) DFT optimized structures of a series of anions adsorbed on Fe surface sites of the NiHCF surface along with the Fe-O and Fe-Cl distances. The values are for the fully intercalated and 50% deintercalated (in parentheses) cases. The corresponding adsorption energies are presented in **Table 1**.

Hypothesizing that the degradation process is initiated by the adsorption of anions from the electrolyte on the metal centers of the NiHCF surface, the adsorption strength and, therefore, the impact of the individual anions should differ considering their distinct geometry, size,

charge density and polarity. To quantify this effect, we examine the adsorption energetics for ClO_4^-, NO_3^-, Cl^-, CH_3COO^-, SO_4^{2-} and OH^-. **Table 1** lists the computed binding energies for the anions adsorbed at the Fe and Ni surface sites of NiHCF. It is seen that the surface affinity for anions is very strong, assuming specific adsorption with preferential binding to Fe centers in both intercalated and deintercalated NiHCF. To confirm that these results do not depend on a particular choice of the *U* values in our computational scheme, we also ran a series of plain DFT calculations (see **Table S2**). It appears striking to see that even perchlorate, which is known as a weak adsorbate on metals[35], yields considerably high adsorption energies when adsorbed over Fe. **Figure 5d** shows the atomic configurations of the anions adsorbed on the Fe sites of the NiHCF surface. It can be observed that the stronger adsorbed anions (SO_4^{2-} and OH^-) are characterized by shorter interfacial distances than the weaker adsorbed species. Also, the distances are decreased upon deintercalation, in agreement with the overall more positive charge on the host Fe sites after Na removal (see **Table S3**). Endorsing our experimental studies, these computational results support the proposed mechanism of anions dictating the kinetics of the interfacial charge and mass transport by adsorption on the electrode surface during (de)intercalation of alkali metal cations in PBAs.[18,19,20]

Table 1. DFT computed adsorption energies (E_{ads}) for a series of electrolyte anions adsorbed over Fe and Ni surface sites of intercalated and 50% deintercalated NiHCF. The corresponding distances between the adsorbates and the surface metal centers are provided in **Figure 5d**.

	Intercalated		**50% deintercalated**	
Adsorbate	**E_{ads} (Fe), eV**	**E_{ads} (Ni), eV**	**E_{ads} (Fe), eV**	**E_{ads} (Ni), eV**
OH^-	-2.87	-1.41	-2.91	-1.58
Cl^-	-2.73	-2.04	-2.52	-1.74
SO_4^{2-}	-3.54	-1.84	-3.55	-2.49
ClO_4^-	-2.65	-2.35	-2.47	-2.25
NO_3^-	-1.29	-1.35	-1.57	-1.23
CH_3COO^-	-1.89	-1.26	-1.57	-1.28

It is also seen from **Table 1** that SO_4^{2-} and OH^- anions are characterized by the strongest and CH_3COO^-, NO_3^- and ClO4$^-$ by the weakest adsorption to the NiHCF surface. The calculated adsorption energetics appears to qualitatively correlate with the decreasing stability of NiHCF from the perchlorate to sulfate electrolytes upon cycling. The exact dissolution pathways of the specific electrode constituents are certainly too complicated to be entirely unveiled by our simplified approach, but it clearly identifies anion attack to catalyze the degradation process *via* specific adsorption and subsequent metal extraction by breaking the lattice bonds. Considering the obtained strong (chemi)/adsorption energies in the order of 2 – 3.5 eV, ligand exchange leading to the formation and dissolution of, e.g., $[Fe^{III}(CN)_5OH]^{3-}$ in the alkaline case cannot be excluded.

However, these DFT results cannot explain the experimentally observed low stability of NiHCF in 0.25 M sodium acetate, as one should in fact expect the slowest degradation rate according to the weak anion adsorption in this case. We suppose that the unexpected detrimental role of CH_3COO^- is related to its considerably higher basic strength ($pK_b = 9.24$)[36] compared to the other investigated anions. Even though the sodium acetate electrolyte was adjusted to a neutral pH = 6.1, this only reflects an overall statistical quantity. On a molecular level, hydrolysis due to the de-protonation of H_2O and subsequent CH_3COOH formation will result in the local appearance of free OH^-. This in turn accelerates the degradation of the electrode if the process occurs close to its surface. In contrast to the pure NaOH case, this will not lead to the formation of NiO_x (as it is not stable at medium pH), but to the dissolution of active material. Extrapolating these findings, a low stability of PBAs in other carboxylic anions corresponding to weak acids should be expected. Furthermore, this argument allows the explanation of the previously published low stability observed for PBA electrodes in 1 M $Mg(ClO_4)_2$ solutions.[37] Besides Mg^{2+}, the initial dissolution of NiHCF electrodes was also observed in other divalent metal nitrate electrolytes (Ca^{2+}, Sr^{2+}).[38] Assuming a similar

mechanism, local hydrolysis and $X(OH)_2$ precipitation (with X = Mg, Ca, Sr) might result in free H_3O^+, which can in turn initiate the acidic degradation pathway. In contrast to the mixed H_3O^+/Na^+ electrolyte, we expect that H_3O^+ is a preferred intercalate over Mg^{2+} and therefore catalyzes the electrode dissolution.

Lastly, we investigate the effect of the electrolyte concentration on electrode stability. It has been shown in previous works on PBAs that the dissolution of active material can be suppressed by increasing the concentration of the electrolyte towards so-called water-in-salt electrolytes.[17,33,39,40] $NaClO_4$ has proven to be a promising candidate for this approach as concentrations beyond 10 M are feasible for this salt.[39,41] **Figure 6** shows the stability of NiHCF electrodes for varying concentrations from 0.25 M to 8 M $NaClO_4$. The stability slightly decreases when raising the concentration from 0.25 M to 1M, while a significant stabilization of the material can be observed above 2 M with almost no degradation for an 8 M $NaClO_4$ solution. For the super-concentrated electrolytes, the material hydrolysis is effectively suppressed through the absence of free water molecules, as these are excessively incorporated in the ions' solvation shells due to the strong hydration of the salt. In fact, only a very few water molecules exist per one sodium perchlorate molecule causing a vanishing uptake capability for dissolved electrode constituents.[42] Furthermore, the sluggish diffusion dynamics for dissolved electrode constituents in the electrolyte bulk strongly inhibit electrode degradation in such water-in-salt systems.[43] For the low to medium concentrated solutions, we assign the slight decrease of the stability to the effect of the ClO_4^- anion. Even though this species was found to adsorb on the electrode surface only weakly, its increased activity at higher concentrations could lead to a stronger degradation of the active material. However, beyond a concentration of 2 M the stabilizing crowding effect of the electrolyte prevails.

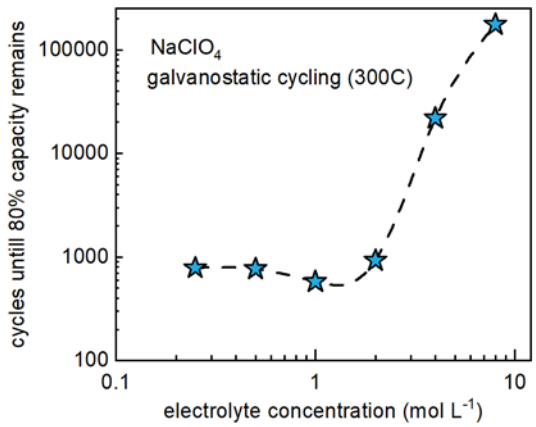

Figure 6. Stability of NiHCF in varying concentrations of $NaClO_4$ during galvanostatic cycling (300C). The datapoints show the number of cycles after a loss of 20% capacity. For the 4 M and 8 M solutions the stability was extrapolated based on the measured capacity losses of 2.6% after 2840 cycles and 1.2% after 10 500 cycles.[17] The dashed line serves as a guide to the eye.

Summary and Conclusions

In this work, the governing mechanisms driving the degradation of model $Na_2Ni[Fe(CN)_6]$ electrodes based on the electrolyte composition were elucidated by a combined experimental and theoretical approach. DFT calculations for the anions commonly used in electrochemical systems showed that the NiHCF surface has a significant affinity for anion adsorption with binding energies up to ~3.5 eV. This finding emphasizes a non-negligible role of anion specific adsorption in the complex mechanism of interfacial mass and charge transfer during the intercalation of alkali metal cations. It is shown that the surface Fe-sites are more favorable for anion adsorption than Ni-sites, forming the following trend for the adsorption strength of anions on Fe (surface layer atoms): $SO_4^{2-} > OH^- > Cl^- > ClO_4^- > CH_3COO^- > NO_3^-$. The anion adsorption characteristics allow to explain the drastic differences in the stability of PBA electrodes, confirming the experimentally determined higher stability in the presence of weakly

adsorbing anions like ClO_4^- and NO_3^- compared to the strongly adsorbing SO_4^{2-} and OH^-. Considering the special role of hydroxide, the respective basic strength of the anions also has to be taken into account, excluding the acetate anion from stable electrode cycling. Whereas a benign acidification (pH ~ 2 – 3) of the electrolyte generally helps to increase the stability due to the decreased OH^- activity, an overwhelming availability and intercalation of H_3O^+ causes a fast deterioration of the Ni – N ≡ C – Fe bond due to protonation of the N-sites within the crystal structure and subsequent electrode dissolution.

We point out, however, that it is not straightforward to predict the stability of PBAs in aqueous environments by a single generalized mechanism. Overall, the material stability is determined by a complex interplay of competing processes involving anion attack *via* strong adsorption on the electrified interface, specifically OH^- induced hydrolysis, and protonation of the CN-group in the presence of hydronium. Therefore, the exact composition of the electrolyte should be carefully considered for achieving a long material lifetime as the solution pH, salt concentration and the involved anion determine its resistance against degradation. These findings should be of great importance in optimizing electrochemical systems based on PBA materials, interpreting experimental results, and elucidation of the advanced models of the electrified PBA/electrolyte interfaces.

Acknowledgements

We want to thank the German Research Foundation (DFG) under Germany's excellence strategy – EXC 2089/1 – 390776260, Germany's excellence cluster "e-conversion". We acknowledge funding support from the National Science Foundation (NSF) through the CBET-1929810 award. This research used the Extreme Science and Engineering Discovery

Environment (XSEDE), which is supported by NSF grant number ACI-1548562, as well as the Liebniz Supercomputing Center (LBZ). XRD and SEM analyses were carried out with the support of CEMNAT Research Infrastructure funded by the Ministry of Education, Youth and Sports of the Czech Republic (projects LM2018103)

Conflict of Interest

The authors declare no conflict of interest.

References

1. J. Han, A. Varzi, S. Passerini. The Emergence of Aqueous Ammonium-Ion Batteries. *Angewandte Chemie International Edition* **2022**, *61*, e202115046.

2. K. Hurlbutt, S. Wheeler, I. Capone, M. Pasta. Prussian Blue Analogs as Battery Materials. *Joule* **2018**, *2*, 1950-1960.

3. B. Xie, B. Sun, T. Gao, Y. Ma, G. Yin, P. Zuo. Recent progress of Prussian blue analogues as cathode materials for nonaqueous sodium-ion batteries. *Coordination Chemistry Reviews* **2022**, *460*, 214478.

4. B. Wang, Y. Han, X. Wang, N. Bahlawane, H. Pan, M. Yan, Y. Jiang. Prussian Blue Analogs for Rechargeable Batteries. *iScience* **2018**, *3*, 110-133.

5. Y. Avila, P. Acevedo-Peña, L. Reguera, E. Reguera. Recent progress in transition metal hexacyanometallates: From structure to properties and functionality. *Coordination Chemistry Reviews* **2022**, *453*, 214274.

6. Y. Matos-Peralta, M. Antuch. Prussian blue and its analogs as appealing materials for electrochemical sensing and biosensing. *Journal of the Electrochemical Society* **2019**, *167*(3), 037510.

7. S. M. Chen, C. Y. Liou, R. Thangamuthu. Preparation and Characterization of Mixed-Valent Nickel Oxide/Nickel Hexacyanoferrate Hybrid Films and Their Electrocatalytic Properties. *Electroanalysis: An International Journal Devoted to Fundamental and Practical Aspects of Electroanalysis* **2007**, *19*(23), 2457-2464.

8. X. Su, Y. Wang, J. Zhou, S. Gu, J. Li, S. Zhang. Operando Spectroscopic Identification of Active Sites in NiFe Prussian Blue Analogues as Electrocatalysts: Activation of Oxygen Atoms for Oxygen Evolution Reaction. *J. American Chemical Society* **2018**, *140*, 11286–11292.

9. H. Zhang, P. Li, S. Chen, F. Xie, D.J. Riley. Anodic Transformation of a Core-Shell Prussian Blue Analogue to a Bifunctional Electrocatalyst for Water Splitting. *Advanced Functional Materials* **2021**, *31*, 2106835.

10. T. Shibata, Y. Moritomo. Quick Response of All Solid Electrochromic Device. *Appl. Phys. Express* **2009**, *2*, 105502.

11. W.-J. Li, S. Xue, S. Watzele, S. Hou, J. Fichtner, A.L. Semrau, L. Zhou, A. Welle, A.S. Bandarenka, R.A. Fischer. Advanced bifunctional oxygen reduction and evolution electrocatalyst derived from surface-mounted metal-organic frameworks. *Angewandte Chemie International Edition* **2020**, *59*, 5837-5843.

12. Y. Yang, C. Brownell, N. Sadrieh, J. May, A. Del Grosso, D. Place, P. Faustino, *et al*.. Quantitative measurement of cyanide released from Prussian Blue. *Clinical Toxicology* **2007**, *45*(7), 776-781.

13. D. E. Stilwell, K. H. Park, M. H. Miles. Electrochemical studies of the factors influencing the cycle stability of Prussian Blue films. *Journal of applied electrochemistry* **1992**, *22*(4), 325-331.

14. H. Mimura, J. Lehto, R. Harjula. Chemical and thermal stability of potassium nickel hexacyanoferrate(II). *Journal of nuclear science and technology* **1997**, *34*(6), 582-587.

15. P. Marzak, J. Yun, A. Dorsel, A. Kriele, R. Gilles, O. Schneider, A. S. Bandarenka. Electrodeposited $Na_2Ni[Fe(CN)_6]$ thin-film cathodes exposed to simulated aqueous Na-ion battery conditions. *The Journal of Physical Chemistry C* **2018**, *122*(16), 8760-8768.

16. T. R. Cataldi, R. Guascito, A. M. Salvi. XPS study and electrochemical behaviour of the nickel hexacyanoferrate film electrode upon treatment in alkaline solutions. *Journal of Electroanalytical Chemistry* **1996**, *417*(1-2), 83-88.

17. X. Lamprecht, F. Speck, P. Marzak, S. Cherevko, A.S. Bandarenka. Electrolyte effects on the stabilization of Prussian blue analog electrodes in aqueous sodium-ion batteries. *ACS Applied Materials and Interfaces* **2022**, *14*, 3515-3525.

18. D. Scieszka, C. Sohr, P. Scheibenbogen, P. Marzak, J. Yun, Y. Liang, J. Fichtner, A.S. Bandarenka. Multiple potentials of maximum entropy of a $Na_2Co[Fe(CN)_6]$ battery electrode material: does the electrolyte composition control the interface? *ACS Applied Materials and Interfaces* **2018**, *10*, 21688–21695.

19. E. Ventosa, B. Paulitsch, P. Marzak, J. Yun, F. Schiegg, T. Quast, A.S. Bandarenka. The mechanism of the interfacial charge and mass transfer during intercalation of alkali metal cations. *Advanced Science* **2016**, *3*, 1600211.

20. J. Yun, J. Pfisterer, A.S. Bandarenka. How simple are the models of Na-intercalation in aqueous media? *Energy & Environmental Science* **2016**, *9*, 955-961.

21. S. J. Gerber, E. Erasmus. Electronic effects of metal hexacyanoferrates: An XPS and FTIR study. *Materials Chemistry and Physics* **2018**, *203*, 73-81.

22. F. Scholz, A. Dostal, A. The formal potentials of solid metal hexacyanometalates. *Angewandte Chemie International Edition* **1996**, *34*(23-24), 2685-2687.

23. B. Paulitsch, Y. Yun, A. S. Bandarenka. Electrodeposited $Na_2VO_x[Fe(CN)_6]$ films as a cathode material for aqueous Na-ion batteries. *ACS Applied Materials & Interfaces* **2017**, *9*(9), 8107-8112.

24. W. Zhang, Y. Zhao, V. Malgras, Q. Ji, D. Jiang, R. Qi, M. Hu, *et al*. Synthesis of monocrystalline nanoframes of prussian blue analogues by controlled preferential etching. *Angewandte Chemie International Edition* **2016**, *55*(29), 8228-8234.

25. Y. Zhu, B. Wang, Q. Gan, Y. Wang, Z. Wang, J. Xie, Z. Lu, *et al*. Selective edge etching to improve the rate capability of Prussian blue analogues for sodium ion batteries. *Inorganic Chemistry Frontiers* **2019**, *6*(6), 1361-1366.

26. M. Hu, S. Furukawa, R. Ohtani, H. Sukegawa, Y. Nemoto, J. Reboul, Y. Yamauchi, *et al*. Synthesis of Prussian blue nanoparticles with a hollow interior by controlled chemical etching. *Angewandte Chemie International Edition* **2012**, *51*(4), 984-988.

27. M. Hu, A. A. Belik, M. Imura, Y. Yamauchi. Tailored design of multiple nanoarchitectures in metal-cyanide hybrid coordination polymers. *Journal of the American Chemical Society* **2013**, *135*(1), 384-391.

28. Z. Li, J. Zhang, T. Mu, J. Du, Z. Liu, B. Han, J. Chen. Preparation of polyvinylpyrrolidone-protected Prussian blue nanocomposites in microemulsion. *Colloids and Surfaces A: Physicochemical and Engineering Aspects* **2004**, *243*(1-3), 63-66.

29. X. Wu, J. J. Hong, W. Shin, L. Ma, T. Liu, X. Bi, X. Ji, *et al*. Diffusion-free Grotthuss topochemistry for high-rate and long-life proton batteries. *Nature Energy* **2019**, *4*(2), 123-130.

30. C. D. Wessells, S. V. Peddada, R. A. Huggins, Y. Cui. Nickel hexacyanoferrate nanoparticle electrodes for aqueous sodium and potassium ion batteries. *Nano letters* **2011**, *11*(12), 5421-5425.

31. C. D. Wessells, R. A. Huggins, Y. Cui. Copper hexacyanoferrate battery electrodes with long cycle life and high power. *Nature communications* **2011**, *2*(1), 1-5.

32. R. R. Gaddam, L. Katzenmeier, X. Lamprecht, A. S. Bandarenka. Review on physical impedance models in modern battery research. *Physical Chemistry Chemical Physics* **2021**, *23*(23), 12926-12944.

33. X. Lamprecht, P. Marzak, A. Wieczorek, N. Thomsen, J. Kim, B. Garlyyev, Y. Liang, A. S. Bandarenka, J. Yun. High Voltage and Superior Cyclability of Indium Hexacyanoferrate Cathodes for Aqueous Na-ion Batteries Enabled by Superconcentrated NaClO4 Electrolytes. *Energy Advances* **2022**, *DOI: 10.1039/D2YA00130F*

34. R. Bors, J. Yun, P. Marzak, J. Fichtner, D. Scieszka, A. S. Bandarenka. Chromium (II) hexacyanoferrate-based thin films as a material for aqueous alkali metal cation batteries. *ACS omega* **2018**, *3*(5), 5111-5115.

35. M. Kasuya, T. Sogawa, T. Masuda, T. Kamijo, K. Uosaki, K. Kurihara. Anion adsorption on gold electrodes studied by electrochemical surface forces measurement. *The Journal of Physical Chemistry C* **2016**, *120*(29), 15986-15992.

36. D. R. Lide. CRC Handbook of Chemistry and Physics, 84th Edition, Section 8. *CRC Press LLC* **2004**.

37. P. Marzak, M. Kosiahn, J. Yun, A.S. Bandarenka. Intercalation of Mg^{2+} into electrodeposited Prussian Blue Analogue thin films from aqueous electrolytes. *Electrochimica Acta* **2019**, *307*, 157-163.

38. R.Y. Wang, C.D. Wessells, R.A. Huggins, Y Cui. Highly reversible open framework nanoscale electrodes for divalent ion batteries. *Nano letters* **2013**, *13*(11), 5748-5752.

39. M. Pasta, C. D. Wessells, N. Liu, J. Nelson, M. T. McDowell, R. A. Huggins, Y. Cui, *et al.* Full open-framework batteries for stationary energy storage. *Nature communications* **2014**, *5*(1), 1-9.

40. J. Yun, F. A. Schiegg, Y. Liang, D. Scieszka, B. Garlyyev, A. Kwiatkowski, A. S. Bandarenka, *et al*. Electrochemically Formed $Na_xMn[Mn(CN)_6]$ Thin Film Anodes Demonstrate Sodium Intercalation and Deintercalation at Extremely Negative Electrode Potentials in Aqueous Media. *ACS Applied Energy Materials* **2017**, *1*(1), 123-128.

41. D. Reber, R. Grissa, M. Becker, R. S. Kühnel, C. Battaglia. Anion Selection Criteria for Water-in-Salt Electrolytes. *Advanced Energy Materials* **2021**, *11*(5), 2002913.

42. H. Tomiyasu, H. Shikata, K. Takao, N. Asanuma, S. Taruta, Y. Y. Park. An aqueous electrolyte of the widest potential window and its superior capability for capacitors. *Scientific Reports* **2017**, *7*(1), 1-12.

43. L. Chen, W. Sun, K. Xu, Q. Dong, L. Zheng, J. Wang, H. Chen, *et al*. How Prussian Blue Analogues Can Be Stable in Concentrated Aqueous Electrolytes. *ACS Energy Letters* **2022**, *7*(5), 1672-1678.